Materials Today Communications 30 (2022) 103091

Contents lists available at ScienceDirect

Materials Today Communications

journal homepage: www.elsevier.com/locate/mtcomm

Reusable hybrid nanocomposites for clean degradation of dye waste under visible light

Claudiu Colbea [a,b], Petruta Oancea [a], Mihaela Puiu [a,1], Toma Galaon [c], Adina Raducan [a,1,*]

[a] Department of Physical Chemistry, University of Bucharest, 4-12 Elisabeta Blvd., 030018 Bucharest, Romania
[b] National Institute for Laser, Plasma and Radiation Physics, RO 76900 Bucharest-Magurele, Romania
[c] National Research and Development Institute for Industrial Ecology – INCD-Ecoind, 71-73 Drumul Podu Dambovitei, Bucharest, Romania

ARTICLE INFO

Keywords:
Photosensitized TiO_2
Azo dyes oxidation
Photocatalysis: kinetics

ABSTRACT

Herein we report on the degradation performance of three phthalocyanine-photosensitized TiO_2 nanocomposites on waste dyes such as Ponceau 4R, Sella Fast Black, Congo Red, Select Brown, Indigo Carmine, Brilliant Blue, Fuchsin, Fluorescein and Naphthol Yellow S. All experiments were carried on at neutral pH, in ambient conditions, requiring only visible light and no additional oxidants. Chlorinated copper (II) α-phthalocyanine (αClCuPc), copper (II) β-phthalocyanine (βCuPc), and tetra-sulfonated copper (II) β-phthalocyanine (βSCuPc) increased the decolourization efficiency of TiO_2 from moderate to high degrees, *i.e.*, 30–100%, even for recalcitrant azo-dyes such as Ponceau 4R, Sella Fast Black, Congo Red and Select Brown. Moreover, the photosensitized catalysts display good thermal, operational stability, and reusability, providing total organic carbon (TOC) removal above 50% within 180 min in batch conditions. The reactive oxygen species were generated in the presence of dissolved oxygen, through the activation of phthalocyanine/TiO_2 and it can be combined further with enzymatic/microbial treatment to achieve total mineralization.

1. Introduction

The treatment of refractory organics from industrial effluents is a continuously expanding field of research worldwide, due to the systematic pollution of aqueous environments during the past decades [1]. Among other pollutants discarded in surface waters, industrial dyes are major threats to the integrity of aquatic ecosystems. It is estimated that around 7×10^5 tons of dyestuffs are produced annually and 280,000 tons of industrial dyes are released into aquatic surroundings via textile effluents [2]. Textile dyes are intended to resist degradation, are chemically stable, non-biodegradable and exhibit toxic and carcinogenic features [3,4]. They adhere on compatible surfaces trough mechanical retention, physical adsorption, covalent binding or chelation [5]. Conventional biological wastewater procedures may not be effective in treating dye wastewater because they generate significant amounts of sludge or cause secondary pollution due to the formation of by-products. Therefore, novel treatment technologies dealing with these issues are currently in high demand. Advanced oxidation processes (AOPs) are the recognized "clean" technologies for recalcitrant dyes destruction or for transformation into less harmful chemicals [6,7]. Almost all AOPs are based on the production of hydroxyl radical, a powerful oxidizing species (with E_0 varying between +1.8 and + 2.7 V *vs.* NHE) [8], which can degrade non-selectively refractory organics with rate constants of around 10^9 L mol^{-1} s^{-1} [9]. Among AOPs, great attention has been paid to photocatalytic treatments, as they are prominent environment-friendly and sustainable technologies [10]. Most photocatalytic treatments of wastewater using photoactive materials are based on TiO_2-generated reactive oxygen species (ROS). TiO_2 is probably the most investigated photocatalyst, owing to its enhanced photo-activity, low cost, decreased toxicity and good chemical and thermal stability [11]. Besides these unique physical and chemical properties, nanosized anatase (1–100 nm) displays also high surface to volume ratio and consequently high degrees of dye adsorption onto catalyst's surface [12]. However, the catalytic efficiency of TiO_2 is limited for practical applications mostly because the photo-generated charge carriers recombine fast due to a relatively wide band gap (3.2 eV), therefore ultraviolet (UV) light (wavelength up to 387 nm) is required [13]. Hence, the photocatalytic efficiency of TiO_2 could be improved by shifting its optical response to the visible (VIS) range. [10,14]. Dye-sensitized photocatalysis starts with the light absorption of dye

* Corresponding author.
E-mail address: adina.raducan@g.unibuc.ro (A. Raducan).
[1] These authors contributed equally.

https://doi.org/10.1016/j.mtcomm.2021.103091
Received 26 July 2021; Received in revised form 9 December 2021; Accepted 15 December 2021
Available online 17 December 2021

to reach an excited state. Depending on its redox environment, the dye can transfer (in most cases) or to get an electron, improving the electron/hole separation [15,16]. If the redox potential of the excited state is lower than the conduction band (CB) of TiO_2 (more negative), then an electron can be injected from the excited state into the CB of TiO_2 [14, 17] (Eqs. (1) and (2)).

$$Dye + h\vartheta \rightarrow Dye^* \quad (1)$$

$$Dye^* + TiO_2 \rightarrow Dye^{*+} + TiO_2(e^-) \quad (2)$$

The injected electron reacts with surface adsorbed O_2 to yield superoxide radical $O_2^{\cdot-}$, which in turn produces $HOO^{\cdot}$ through protonation (Eqs. (3) and (4)) [18]. The formation of H_2O_2 and the subsequent generation of $HO^{\cdot}$ (Eqs. (5) and (6)) [19,20] are the main steps yielding to the degradation of organic pollutants.

$$TiO_2(e^-) + O_2 \rightarrow TiO_2 + O_2^{\cdot-} \quad (3)$$

$$O_2^{\cdot-} + H^+ \rightarrow HOO\bullet \quad (4)$$

$$2HOO\bullet \rightarrow H_2O_2 + O_2 \quad (5)$$

$$H_2O_2 + e^- \rightarrow HO^- + HO\bullet \quad (6)$$

The photoinduced degradation with dye-sensitized TiO_2 nanocatalysts under visible light irradiation has been recently tested onto several low molecular weight targets such as 4-chlorophenol [17], 2, 4-dichlorophenol, 2,4,6-trichlorophenol [19] dichlorvos [21] and Methylene Blue [22,23]. However, a major drawback in the case of the dye-sensitized TiO_2 photocatalyst is the fact that the dye molecules are only absorbed onto the TiO_2 surface by physical/chemical adsorption [24]. Therefore, the dye molecules used as sensitizers tend to partially desorb, which can decrease photocatalytic activity during the overall degradation process; thus, the activity can be significantly diminished by the competitive adsorption of other co-existing species [14,25,26]. Since the pollutants usually are present at high concentrations in wastewaters, dye-sensitized photocatalysis may face difficulties maintaining reasonable electron transfer efficiency [26]. Phthalocyanines and their derivatives are able to produce large quantities of singlet oxygen ($^1O_2$) and other ROS under visible light in the presence of dioxygen [27] without requiring other oxidizing agents such as hydrogen peroxide [20,28]. Several phthalocyanines containing transition metal ions (Zn, Co, Cu, Fe) were reported as efficient sensitizing agents for TiO_2 [29–31], due to their strong adsorption onto catalyst's surface. Moreover, carboxylated- and sulfonated phthalocyanines have been reported to cap TiO_2 surface through both electrostatic interactions and chemical binding of acidic groups to Ti–OH moieties onto TiO_2 surface [21,32]. As far as we know, these TiO_2/phthalocyanine nanocomposites are not effective for the degradation of azo dyes, which are long-time persistent hazards in aqueous environment. Therefore, in this study we attempted to synthetize and characterize various TiO_2/phthalocyanine nanomaterials able to efficiently degrade the most common textile dyes found in wastewaters [7,33] through VIS light photoactivation in an environmental-friendly manner. Therefore, Ponceau 4R, Sella Fast Black, Congo Red, Select Brown (azo dyes), Indigo Carmine (indigoid dye), Brilliant Blue, fuchsin (trityl dyes), fluorescein (anthraquinone dye) and Naphtol Yellow S (naphthol dye) were selected for testing the activity of photosensitized catalysts, as they are the most used and often found in wastewaters. The typical amounts of textile dyes present in wastewater are difficult to assess because the textile application methods, even in the same process are different from one industry to another [34]. Yet several excellent works reported dyes level varying from 45 to 600 mg/L [35–37]. The phthalocyanines employed in the photosensitization process were chlorinated copper (II) α-phthalocyanine (αClCuPc), copper (II) β-phthalocyanine (βCuPc) and tetra-sulfonated copper (II) β-phthalocyanine (βSCuPc) (Fig. ES-1).

2. Experimental

2.1. Materials

Titanium (IV) oxide, 99.8% anatase powder, Naphtol Yellow S (Acid Yellow 1, $C_{10}H_4N_2Na_2O_8S$, 75% dye content), Congo Red (Direct Red 28, $C_{32}H_{22}N_6Na_2O_6S_2$, dye content ≥ 35%) and dimethylformamide (DMF) were purchased from Sigma-Aldrich, Germany; commercial copper α-phthalocyanine with 3% organically combined chlorine (αClCuPc, Heliogen Blue K6902) and copper β-phthalocyanine (βCuPc, Heliogen Blue K7090), copper β-phthalocyanine-3,4′,4″,4″ ′-tetrasulfonic acid tetrasodium salt with 85% dye content (C.I. Acid Blue 249) were obtained from BASF, Germany; Commercial dyestuff: Fluorescein (D&C Yellow 7, $C_{20}H_{12}O_5$, 85% dye content), Brilliant Blue (Acid Blue 9, $C_{37}H_{34}N_2Na_2O_9S_3$, 85% dye content), Ponceau 4R (C.I. Acid Red 18, $C_{20}H_{11}N_2Na_3O_{10}S_3$, 85% dye content), Fuchsin (Basic Violet 14, $C_{20}H_{20}ClN_3$, 100% dye content), and Indigo Carmine (C.I. Acid Blue 74, $C_{16}H_8N_2Na_2O_8S_2$, 85% dye content) were obtained from DOW Chemicals, India. Sella Fast Black (Acid Black 210, $C_{34}H_{25}K_2N_{11}O_{11}S_3$), and Select Brown (Acid Brown 98, $C_{48}H_{39}FeN_{15}O_{21}S_3$) were purchased from TFL Ledertechnik GmbH, Germany.

2.2. Synthesis of TiO_2/phthalocyanine nanocomposites

Each synthesis was performed by vigorous mixing of 300 mL 3% (w/w) TiO_2 suspension in water with 10 mL phthalocyanine solution (2 mg/mL) in DMF [38]. The dispersions were gently mixed and stirred further for 6 h. The drying process was carried out in a rotary evaporator at 60 °C. The low drying temperature was chosen for organic compounds preservation. This drying technique was chosen over the filtration method because the TiO_2 nanoparticles could pass through the filter resulting in mass loss.

2.3. Investigating photocatalyst features

The TiO_2/phthalocyanine nanocomposites were characterized *via* X-Ray Diffraction (XRD), Attenuated total reflectance Fourier-transform infrared spectroscopy (ATR-FTIR), Diffuse reflectance (DR) ultraviolet/visible (UV/VIS) spectroscopy and Scanning Electron Microscopy (SEM).

For XRD analysis, an Brucker D8 Advance XRD (Massachusetts, U.S.), (0.02°/min steps and 0.7 s integration time) was used and phase content was verified by two software approaches: PDF Cards online via the included software, using the reference database ICDD: International Centre for Diffraction Data and MAUD [39] software which requires the CIF data files (Crystallography.net source) and it is based on RITA/R-ISTA method. Both approaches returned the same result. The DR absorption spectra were measured on an UV- 3600 SHIMADZU UV–VIS–NIR spectrophotometer MPC-3100 (Japan), considering the limiting case of an infinitely thick sample thickness and sample holder have no influence on the value of reflectance (R). ATR FTIR spectra of the compounds were recorded on a PerkinElmer Spectrum One FTIR spectrophotometer (Massachusetts, U.S.) with attenuated total reflectance. (ATR) sampling accessory was used for infrared (IR) data collection. SEM measurements of synthesized catalysts were investigated using a Thermo Scientific Quattro S microscope with an accelerating voltage of 8 kV, with a spot size of 200; images were obtained with a spot size of 200 at the magnification ranges of 10000× and 20000× without coating.

2.4. Differential scanning calorimetry (DSC) and thermogravimetric analysis (TGA)

DSC analysis was performed in a Perkin Elmer Diamond DSC calorimeter (Massachusetts, U.S.) with a heating rate of 10 °C/minute on a temperature range of (20–200) °C. The measurements were made in

inert argon atmosphere, at a flow rate of 20 mL/minute. The device was calibrated for temperature and enthalpy using high purity indium (T_{fus} = 156.6 °C and $\Delta_{fus}H$ = 28.45 J g^{-1}). 10–20 mg samples were weighed with a Partner XA balance (10 μg precision). The TG experiments were made with a simultaneous thermal analyzer STA 409 PC Luxx (Netzsch, Germany), dynamic inert (nitrogen) atmosphere (analytical grade gasses, with at least 99,999% purity) with a constant flow of about 50 mL/min. A quantity of about 10 mg was tested between 20 and 600 °C at 10 K min^{-1} in aluminum crucibles with pierced caps.

2.5. Photodegradation experiments

The photodegradation of the selected industrial dyes were carried out with and without catalyst in a batch photoreactor. 10 mL of 0.1 mM dye solutions with catalyst were kept in dark for 30 min and then irradiated with a mercury vapour lamp (250 W power, medium pressure), with light emitting in the range 404.5–407.8, 435.8, 546.1 and 570–577 nm for 180 min. The concentration of catalyst was 20 ppm. The temperature was maintained at 25 °C. Samples were withdrawn from the reactor from 30 to 30 min and scanned through UV–VIS measurements.

2.6. Spectrophotometric measurements

The UV–VIS measurements of dye solutions before and after degradation were performed with a JASCO V-530 spectrophotometer (Japan) equipped with a thermostated cell, under continuous stirring, using bi distilled water as reference in all assays.

2.7. Total organic carbon (TOC) assay

TOC analysis of the dye solutions before and after irradiation was performed on an Apollo 900 Combustion TOC Analyzer Teledyne Tekmar, (Ohio, U.S.) with a Nondispersive InfraRed (NDIR) detector for CO_2 (0–20 ppm calibration range). The total combustion of the samples was achieved through the 680 °C combustion catalytic oxidation method. Data processing was performed with the TOC Talk Apollo 9000HS v. 4.2 software.

TOC analysis was performed on solutions of Brilliant Blue, Sella Fast Black and Select Brown containing photocatalysts before and after a 3-hour irradiation, when the calculated decolourization degrees were above 80%.

3. Results and discussions

3.1. Characterization of TiO_2/Pc nanocomposites

The XRD patterns indicate the existence of the anatase phase in TiO_2 (Fig. 1). The particle size was calculated based on Scherrer equation [40]:

$$L = \frac{K\lambda}{\beta\cos\theta} \quad (7)$$

where λ is the wavelength (nm), β is the peak width of the diffraction peak profile at half maximum height resulting from small crystallite size (radians), K is the shape factor which was considered 0.9 in our study and θ is the Bragg angle.

The particles size of roughly 72 nm indicates a nanoparticle domain favouring the photocatalytic process by ensuring a proper dispersion of the nanocomposite in water and a large enough size to be separated by usual techniques.

Neither shift nor modification can be witnessed in the major diffraction peaks of the XRD patterns of TiO_2/CuPc. Based on those outcomes, it appears that the sensitization of the TiO_2 does not alter the crystalline structure of the titania. Similar observation was already

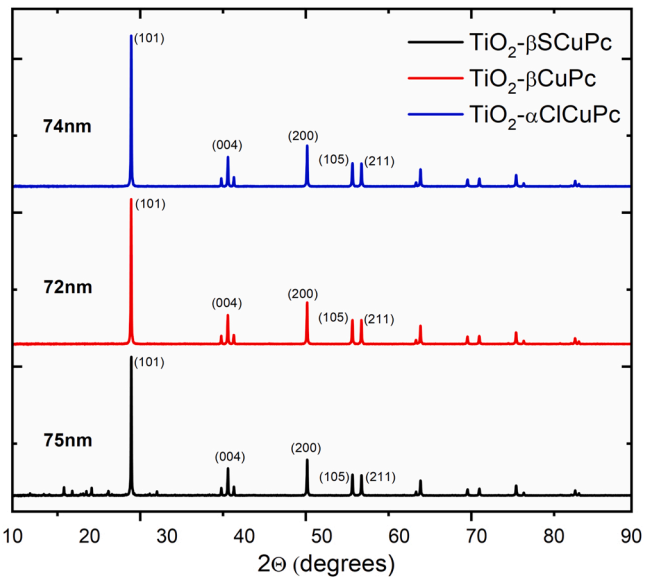

Fig. 1. Patterns of TiO_2 and TiO_2/ phthalocyanine nanocomposites confirming the anatase phase of TiO_2.

reported in several instances [41]. Only for TiO_2/βSCuPc the XRD pattern shows distinctive lines at angles of 20° and 18° which can be assigned to $Ti_{0.75}Cu_{0.25}O_2$ (PDF Card code: 01-081-8477); this indicates that TiO_2 was successfully impregnated with phthalocyanine [42,43]. While the photo-response of bare TiO_2 is restricted to the UV light region, in the absorption spectra of all TiO_2/Pc nanosystems the appearance of new peaks in the region between 400 and 800 nm is observed. The characteristics absorption bands of phthalocyanines (see in Electronic Supplementary Information Fig. ES-2) were observed in the DR-UV–VIS spectra of all three Pc/TiO_2 photocatalysts. Usually, the UV–VIS spectra of Pcs display Q bands located at near IR (600–800 nm), and Soret bands located at near UV (300–400 nm). Both Q and Soret bands correspond to π → π* transitions. Red shifting of absorption spectra was assigned to changes of electron distribution in the tetrabenzo-tetraazaporphyrin ring [44]. Hence the sensitization of TiO_2 with phthalocyanines extends the absorption spectrum to the VIS region [45]. When studying absorption properties, the extinction coefficient E can be expressed as the sum of absorption coefficient K and scattering coefficient S [46,47]. The band gap energies (E_g) were estimated using the Kubelka-Munk equation (Eq. (8)) [48,49] are summarized in Table 1. The limiting case of an infinitely thick sample was considered here, with the assumption that thickness and sample holder have no influence on the reflectance (R). $BaSO_4$ was used as white standard.

$$\frac{K}{S} = \frac{(1 - R_\infty)^2}{2R_\infty} \equiv F(R_\infty) \quad (8)$$

Here, S and K are the so-called K-M scattering and absorption coefficients, $F(R_\infty)$ is the so-called remission or K-M function and the final reflectance $R_\infty = R_{sample}/R_{standard}$. The wavelength was converted in eV by dividing 1240 with the wavelength. The final reflectance was obtained by the square root of the product of the energy and the calculated

Table 1
Band gap energies of the phthalocyanine/TiO_2 nanocomposites resulted from DR-UV–VIS spectra analysis.

Nanomaterial/ Features	TiO_2 anatase	TiO_2/ βSCuPc	/TiO_2/ βCuPc	TiO_2/ αClCuPc
Crystalline structure	Tetragonal	Tetragonal	Tetragonal	Tetragonal
Band Gap (eV)	3.2	2.96	3.2	2.9

reflectance. E_g was calculated as the slope of the linear part of the F *vs* R_∞ plot [49]. As expected, the composites' band gaps were smaller than the reference TiO_2.

The characteristic peaks of phthalocyanines at 1019 nm (pyrrole-N in-plane bending), 1241 nm (C-H bend), 1418 nm (isoindole stretching), 1710 nm (benzene stretching) nm [44] were observed only in the ATR-FTIR spectra of βSCuPc/TiO_2 (Fig. 2) suggesting that αClCuPc and βCuPc were adsorbed only at the surface of TiO_2.

The SEM images of TiO_2/αClCuPc, TiO_2/βCuPc and TiO_2/βSCuPc samples are presented in Fig. 3. For nanocomposites, the micrographs show more clusters of spherical particles indicating particle growth. In TiO_2/αClCuPc, small clusters of particles with an average dimension of 1 μm are noticed, having a more uniform distribution than the other samples. The TiO_2 phase is strongly observed due to the characteristic rounded-shape particles. In TiO_2/βCuPc sample, SEM images reveal an increased accumulation of crystallites with a dense, non-homogeneous morphology due to βCuPc phase. The TiO_2 particles conserved their shape and assembling while βCuPc particles display a tendency to form imprecisely delimited aggregates. For TiO_2/βSCuPc, conglomerates consisting mainly of crystallites with a faceting of submicron and micron sizes spread in the material randomly, having an approximative OY alignment are observed.

The units with diameters larger than 2 μm often contain spherical partial cavities in the volume, which are formed apparently during synthesis. Comparing with pure TiO_2 nanoparticles, the morphology of nanocomposites is almost the same.

3.2. Thermal stability of phthalocyanine/TiO_2 nanocomposites

The thermal properties of Pc/TiO_2 were investigated through DSC and TGA analysis within 20–200 °C. No significant variation assignable to a physical or chemical transition was observed in the DSC curves of αClCuPc/ TiO_2 and βCuPc/ TiO_2, while βSCuPc/TiO_2 displayed several thermal effects at 71, 98, 143 and 167 °C, respectively (Fig. ES-3A). These effects were assigned to the chemical desorption of βSCuPc and to evaporation of residual water and DMF. According to the TGA, the total weight loss was around 2% within 20–200 °C and was probably caused by the evaporation of residual water and DMF (Fig. ES-3B).

3.3. Testing photocatalytic activity

A preliminary test was performed on nine dyes (Fuchsin, Indigo Carmine, Ponceau 4R, Brilliant Blue, Select Brown, Napthol Yellow S, Sella Fast Black, Fluorescein and Congo Red). The experimental setup is presented in Fig. ES-4. Before irradiation, the aqueous solutions of 0.1 mM dye and 20 ppm nanocomposite were kept in dark for 30 min; afterwards, the spectral features of each dye were recorded together with the characteristic absorption peaks (λ = 545 nm for Fuchsin, λ = 609 for Indigo Carmine, λ = 506 nm for Ponceau 4R, λ = 618 nm for Brilliant Blue, λ = 436 nm for Select Brown, λ = 427 nm for Naphthol Yellow S, λ = 605 nm for Sella Fast Black, λ = 490 nm for Fluorescein and λ = 497 nm for Congo Red. It was noticed that a slight decrease of the peak intensities (up to 5%) occurred after 10 min. After this, the dye-containing solutions were irradiated for 30 min in the batch reactor a) without catalyst (photolysis), with b) TiO_2 c) TiO_2/βSCuPc d) TiO_2/βCuPc and e) TiO_2/αClCuPc. The characteristic absorption peaks of each dye were time-monitored, and the decolourization degree/ degradation efficiency was calculated after 30 min (Eq. (9)):

$$D(\%) = \frac{A_0 - A_{30min}}{A_0} \cdot 100 \tag{9}$$

where A_0 is the initial value of the maximum absorbance at specific wavelength and A_{30} is the maximum absorbance after 30 min (Fig. 4). The anthraquinonic dye fluorescein was easily removed through simple photolysis; the decolourization degree of the naphthol Yellow S dye was around 70% in the presence of the bare TiO_2 catalyst. Photosensitization did not increase the decolourization efficiency in the case of Indigo Carmine, but the degradation was significantly enhanced for the two trityl dyes, Fuchsin and Brilliant Blue. Photosensitization with αClCuPc and βCuPc yielded moderate decolourization degrees for two azo dyes (Ponceau 4R and Select Brown) compared with the action of bare catalyst. Sella Fast Black and Congo Red were the most recalcitrant to degradation, yet photosensitization with αClCuPc and βCuPc seemed to slightly increase the activity of the TiO_2 catalyst.

Brilliant Blue, Sella Fast Black, and Select Brown underwent the slowest photo- and photocatalytic degradation in absence of photosensitizers. This made them suitable for a kinetic study in which the irradiation time and catalyst amount can be adjusted.

3.4. Degradation kinetics

It was reported that the photocatalytic degradation of dyes in heterogeneous systems under UV light follows an overall first-order kinetics [50]. In this context, one may expect a similar pattern for irradiation under VIS light. The dependence of the degradation rate on dye concentration is depicted by the Langmuir-Hinshelwood (L-H) equation [51,52]:

$$r_R = -\mathrm{d}[C]/\mathrm{d}t = \frac{kK[C]}{1 + K[C]} \tag{10}$$

where r_R is the rate of dye degradation, k is the degradation rate constant, C is the dye concentration, and K represents the adsorption equilibrium constant. At low dye concentration (millimolar), the

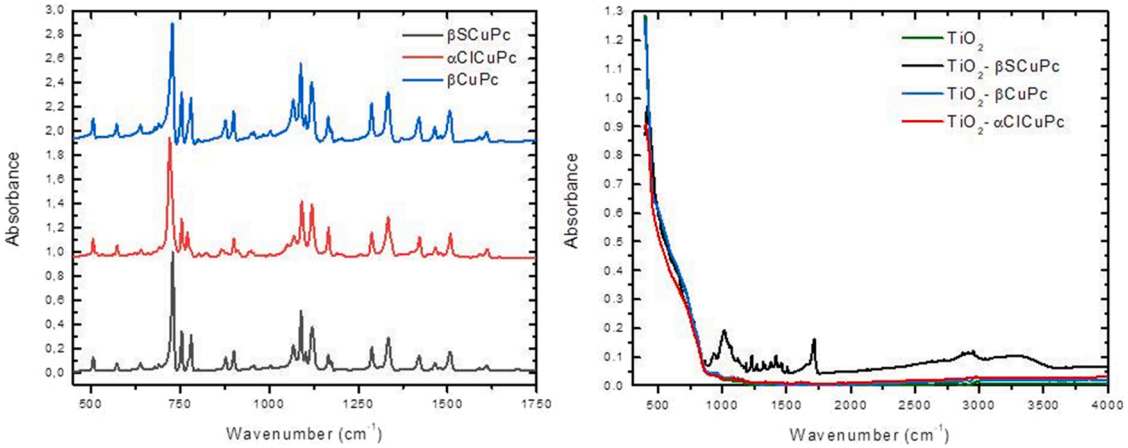

Fig. 2. ATR-FTIR spectra of A) individual phthalocyanines, B) TiO_2/βSCuPcs and reference TiO_2 confirm the successful insertion of βSCuPc in the structure of TiO_2.

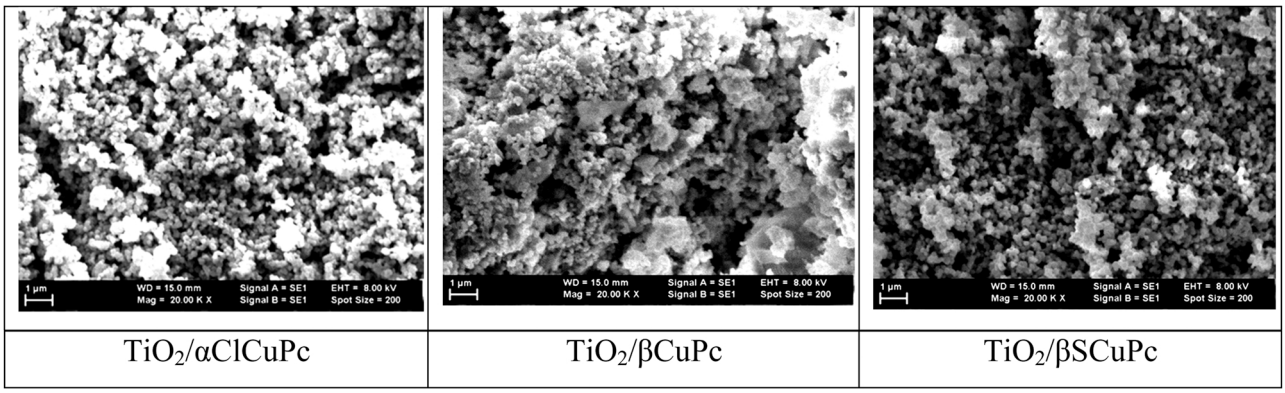

Fig. 3. SEM images of TiO_2/phthalocyanine nanocomposites.

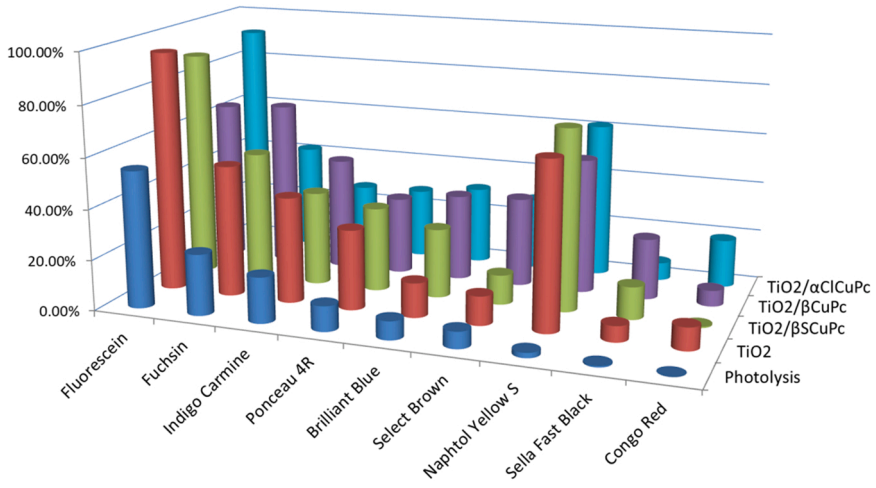

Fig. 4. Degradation efficiency following dye irradiation with VIS light for 30 min: a) without photocatalyst, b) with TiO_2, c) with TiO_2/βCuPc d) with TiO_2/βSCuPc and e) with TiO_2/αClCuPc.

degradation follows an apparent first order kinetics (the term *K[C]* from Eq. (10) becomes negligible with respect to 1):

$$-\frac{d[C]}{dt} = k_{app}[C] \tag{11}$$

and

$$[C]_t = [C]_0 e^{-k_{app}t} \tag{12}$$

where t is time (minutes), $[C]_0$ is the initial concentration and k_{app} represents the apparent rate constant ($k_{app} = k \cdot K$).

0.01 mM dye solutions (Brilliant Blue, Sella Fast Black and Select Brown) were irradiated for 3 h in the presence of 20–150 ppm photosensitized catalysts. The extended kinetic curves absorbance *vs.* irradiation time were used further to validate the apparent first order kinetics and to estimate the k_{app} through non-linear regression analysis (Figs. ES-5–7), according to Eq. (13).

Table 2
Kinetic constants for photodegradation of selected dyes in the presence of TiO_2/phthalocyanine at 25 °C.

Catalyst concentration (ppm)	k_{app} (min^{-1})			
	TiO_2	TiO_2/βSCuPc	TiO_2/βCuPc	TiO_2/αClCuPc
Brilliant Blue				
20	$(3.31 \pm 0.13)\ 10^{-3}$	$(7.09 \pm 0.79)\ 10^{-3}$	$(6.08 \pm 0.22)\ 10^{-3}$	$(4.21 \pm 0.22)\ 10^{-3}$
50	$(6.00 \pm 0.25)\ 10^{-3}$	$(1.62 \pm 0.13)\ 10^{-2}$	$(9.10 \pm 1.22)\ 10^{-3}$	$(5.48 \pm 0.34)\ 10^{-3}$
100	$(7.69 \pm 1.11)\ 10^{-3}$	$(2.25 \pm 0.30)\ 10^{-2}$	$(1.71 \pm 0.13)\ 10^{-2}$	$(1.11 \pm 0.09)\ 10^{-2}$
150	$(7.17 \pm 0.69)\ 10^{-3}$	$(2.28 \pm 0.29)\ 10^{-2}$	$(1.60 \pm 0.12)\ 10^{-2}$	$(1.11 \pm 0.08)\ 10^{-2}$
Select Brown				
20	$(3.42 \pm 0.25)\ 10^{-3}$	$(5.58 \pm 0.49)\ 10^{-3}$	$(9.61 \pm 1.01)\ 10^{-3}$	$(1.64 \pm 0.12)\ 10^{-3}$
50	$(4.98 \pm 0.38)\ 10^{-3}$	$(1.97 \pm 0.20)\ 10^{-2}$	$(1.40 \pm 0.09)\ 10^{-2}$	$(3.55 \pm 0.36)\ 10^{-3}$
100	$(3.32 \pm 0.31)\ 10^{-3}$	$(2.34 \pm 0.26)\ 10^{-2}$	$(3.16 \pm 0.33)\ 10^{-2}$	$(2.02 \pm 0.24)\ 10^{-2}$
150	$(7.54 \pm 0.81)\ 10^{-3}$	$(7.83 \pm 0.82)\ 10^{-3}$	$(3.03 \pm 0.29)\ 10^{-2}$	$(7.01 \pm 0.82)\ 10^{-3}$
Sella Fast Black				
20	$(1.28 \pm 0.13)\ 10^{-3}$	$(1.95 \pm 0.20)\ 10^{-3}$	$(2.15 \pm 0.22)\ 10^{-3}$	$(1.48 \pm 0.13)\ 10^{-4}$
50	$(1.65 \pm 0.19)\ 10^{-3}$	$(3.61 \pm 0.39)\ 10^{-3}$	$(2.21 \pm 0.20)\ 10^{-3}$	$(9.33 \pm 1.02)\ 10^{-4}$
100	$(2.49 \pm 0.31)\ 10^{-3}$	$(8.15 \pm 0.95)\ 10^{-3}$	$(5.59 \pm 0.61)\ 10^{-3}$	$(1.03 \pm 0.13)\ 10^{-3}$
150	$(2.67 \pm 0.28)\ 10^{-3}$	$(8.05 \pm 0.86)\ 10^{-3}$	$(7.34 \pm 0.62)\ 10^{-3}$	$(2.62 \pm 0.32)\ 10^{-3}$

$$[A]_t = [A]_0 e^{-k_{app}t} \quad (13)$$

The estimated rate constants are summarized in Table 2.

The evaluation of the kinetic constants obtained with bare TiO_2 and photosensitized TiO_2 clearly shows that the decolourization rate is increased in the presence of TiO_2/phthalocyanine catalysts. The optimum conditions were met in the presence of 100 ppm catalysts for all dyes. Above this concentration, at 150 ppm the degradation rate seems to slightly decrease. This behaviour may be assigned to the increasing solution opacity which drops the penetration depth of light [53]. TiO_2/βSCuPc increases the decolourization efficiency of Brilliant Blue and Sella Fast Black (one-order magnitude for Brilliant Blue and three-fold for Sella Fast Black compared to TiO_2). TiO_2/βCuPc caused a ten-fold increase of the degradation rate of Select Brown, compared to the performance of bare TiO_2. After 180 min the decolourization was almost complete in the presence 100 ppm photosensitized catalyst (TiO_2/βSCuPc for Brilliant Blue and Sella Fast Black, and TiO_2/βCuPc for Select Brown).

3.5. Quantification of the mineralization level

To assess the efficiency of the photosensitized catalysts on the overall oxidation process TOC analysis was performed because the main concern was the formation of toxic or less biodegradable products. Therefore we monitored TOC for Brilliant Blue, Sella Fast Black and Select Brown before (TOC_0) and after 3-hour irradiation (TOC_∞) in the presence of their most efficient catalysts: TiO_2/βSCuPc for Brilliant Blue and Sella Fast Black and TiO_2/βCuPc for Select Brown. TOC removal was calculated as:

$$\%TOC_{removal} = \frac{TOC_0 - TOC_\infty}{TOC_0} \cdot 100 \quad (14)$$

The results, summarized in Table 3, indicate that the %TOC removal was above 50% for all 3 dyes, confirming the efficiency of the photosensitized catalysts after 3-hour irradiation under visible light without any added oxidant agents.

3.6. Lifespan and stability of photosensitized catalysts

To examine the lifespan and stability of the synthesized TiO_2/phthalocyanine composites, we studied the decolourization efficiency of TiO_2/βSCuPc during a multiple-cycle treatment of Brilliant Blue. The experiments were performed in a 400 mL stirred batch reactor with $5 \cdot 10^{-6}$ M Brilliant Blue. During one cycle, 5 samples of 3 mL were withdrawn from the reactor, *i.e.* 15 mL per cycle (the cycle span is measured from the irradiation start and the total decolorization of the reactant mixture). The samples were then scanned, and their absorbance recorded. The total volume of the solution in reactor remains 385 mL after one cycle, due to samples' recollection. In order to keep the reactor volume constant and to start the next cycle from the same initial dye concentration, 15 mL of solution containing $5 \cdot 10^{-6}$ M dye were further added. The vigorous stirring conditions ensured a homogenous dispersion of the catalyst in the reactant mixture. Since the total volume of recollected samples (15 mL) per cycle represents 3.75% of the reactor volume, we estimated a similar percentage of per-cycle catalyst loss. This assumption is strengthened by the fact the minimal per-cycle catalytic efficiency (CE), calculated as the ratio of the apparent rate constant and the remaining amount of catalyst in solution (m_{cat}) after each cycle (Eq. (15)) remained basically at the same level starting with the second cycle (Fig. ES-8).

$$Catalytic \quad efficiency = \frac{k_{app}}{m_{cat}} \quad (15)$$

where the apparent first-order rate constants were estimated by non-linear regression analysis of the extended kinetic curves, absorbance *vs.* time (Fig. 5).

The initial CE of TiO_2/βSCuPc as defined in Eq. (15), was found 0.425 min^{-1} Kg^{-1}. The 30% drop of CE noticed after the first cycle can be assigned to the aggregation of nanocomposites, as it can be observed by SEM micrographs before and after the reaction (Fig. ES-9). Since no amount of catalyst was added after the first decolorization cycle, the values of k_{app} clearly demonstrate that the minimal CE for a 3.75% catalyst loss per-cycle is due to sample recollection and not to an operational inactivation of the catalyst.

Table 3
Mineralization efficiency of photosensitized catalysts expressed as %TOC removal.

Reactant system	TOC_0 (ppm)	TOC_∞ (ppm)	%TOC removal
Brilliant Blue/TiO_2/βSCuPc	21.5 ± 1.5	11.0 ± 0.8	51.2 ± 3.1
Sella Fast Black/TiO_2/βSCuPc	26.4 ± 0.7	15.6 ± 0.4	59.1 ± 2.8
Select Brown/TiO_2/βCuPc	29.7 ± 1.3	23.2 ± 0.8	78.1 ± 3.6

4. Conclusions

Sensitization of TiO_2 with phthalocyanine *via* wet impregnation has significantly enhanced the photocatalytic activity of TiO_2 under visible light; all photosensitized catalysts used in this study have shown good thermal and operational stability, and good to moderate efficiency in textile dyes' degradation. Moreover, all three TiO_2/αClCuPc, TiO_2/βCuPc and TiO_2/βSCuPc displayed 10-fold increase of the decolourization rate of Brilliant Blue, Sella Fast Black and Select Brown compared to the simple TiO_2. Decolourization of dyes was almost complete within 180 min, while the TOC removal of degradation resistant dyes such as Brilliant Blue (trityl) and Sella Fast Black (azo dye) was within 50–60%. Technologies using phthalocyanine-photosensitized catalysts can be costly-efficient, environmentally friendly alternative to current treatments of surface waters polluted with industrial dyes.

CRediT authorship contribution statement

Claudiu Colbea: Methodology, Formal analysis, Writing – original draft. **Petruța Oancea:** Methodology, Formal analysis, Validation, Investigation, Writing – review & editing. **Mihaela Puiu:** Formal analysis, Writing – original draft, Writing – review & editing. **Toma Galaon:** Methodology, Investigation, Formal analysis, Writing – original draft. **Adina Răducan:** Conceptualization, Methodology, Formal analysis, Investigation, Writing – review & editing, Supervision, Project

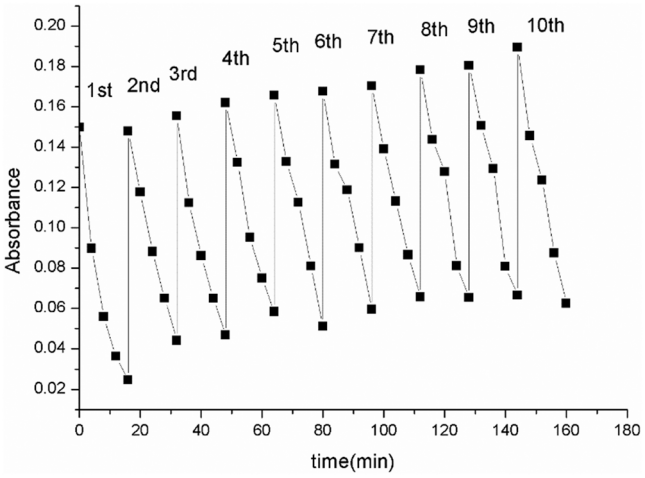

Fig. 5. Time evolution of dye absorbance in the presence of TiO_2/βSCuPc following catalyst multiple recycling ($5\ 10^{-6}$ M Brilliant Blue under VIS irradiation, 100 ppm TiO_2/βSCuPc, 10 cycles).

administration.

Declaration of Competing Interest

The authors declare that they have no known competing financial interests or personal relationships that could have appeared to influence the work reported in this paper.

Appendix A. Supporting information

Supplementary data associated with this article can be found in the online version at doi:10.1016/j.mtcomm.2021.103091.

References

[1] B. Petrie, R. Barden, B. Kasprzyk-Hordern, A review on emerging contaminants in wastewaters and the environment: current knowledge, understudied areas and recommendations for future monitoring, Water Res. 72 (2015) 3–27.

[2] Z. Eren, N.H. Ince, Sonolytic and sonocatalytic degradation of azo dyes by low and high frequency ultrasound, J. Hazard. Mater. 177 (2010) 1019–1024.

[3] A. Asghar, A.A. Abdul Raman, W.M.A. Wan Daud, Advanced oxidation processes for in-situ production of hydrogen peroxide/hydroxyl radical for textile wastewater treatment: a review, J. Clean. Prod. 87 (2015) 826–838.

[4] S.U. Jadhav, M.U. Jadhav, A.N. Kagalkar, S.P. Govindwar, Decolorization of Brilliant Blue G dye mediated by degradation of the microbial consortium of Galactomyces geotrichum and Bacillus sp, J. Chin. Inst. Chem. Eng. 39 (2008) 563–570.

[5] A. Bafana, S.S. Devi, T. Chakrabarti, Azo dyes: past, present and the future, Environ. Rev. 19 (2011) 350–371.

[6] G. Boczkaj, A. Fernandes, Wastewater treatment by means of advanced oxidation processes at basic pH conditions: a review, Chem. Eng. J. 320 (2017) 608–633.

[7] L. Bilińska, M. Gmurek, Novel trends in AOPs for textile wastewater treatment. Enhanced dye by-products removal by catalytic and synergistic actions, Water Resour. Ind. 26 (2021), 100160.

[8] A.R. Ribeiro, O.C. Nunes, M.F.R. Pereira, A.M.T. Silva, An overview on the advanced oxidation processes applied for the treatment of water pollutants defined in the recently launched Directive 2013/39/EU, Environ. Int. 75 (2015) 33–51.

[9] J. Hoigné, Chemistry of aqueous ozone and transformation of pollutants by ozonation and advanced oxidation processes, in: J. Hrubec (Ed.), Quality and Treatment of Drinking Water II, Springer Berlin Heidelberg, Berlin, Heidelberg, 1998, pp. 83–141.

[10] D. Ayodhya, G. Veerabhadram, A review on recent advances in photodegradation of dyes using doped and heterojunction based semiconductor metal sulfide nanostructures for environmental protection, Mater. Today Energy 9 (2018) 83–113.

[11] A.V. Emeline, V.N. Kuznetsov, V.K. Ryabchuk, N. Serpone, Heterogeneous photocatalysis: basic approaches and terminology, in: S.L. Suib (Ed.), New and Future Developments in Catalysis, Elsevier, Amsterdam, 2013, pp. 1–47.

[12] C. Beer, R. Foldbjerg, Y. Hayashi, D.S. Sutherland, H. Autrup, Toxicity of silver nanoparticles—Nanoparticle or silver ion? Toxicol. Lett. 208 (2012) 286–292.

[13] R. Asahi, Y. Taga, W. Mannstadt, A.J. Freeman, Electronic and optical properties of anatase TiO2, Phys. Rev. B 61 (2000) 7459–7465.

[14] H. Dong, G. Zeng, L. Tang, C. Fan, C. Zhang, X. He, Y. He, An overview on limitations of TiO2-based particles for photocatalytic degradation of organic pollutants and the corresponding countermeasures, Water Res. 79 (2015) 128–146.

[15] F. Kiriakidou, D.I. Kondarides, X.E. Verykios, The effect of operational parameters and TiO2-doping on the photocatalytic degradation of azo-dyes, Catal. Today 54 (1999) 119–130.

[16] C. Diaz-Uribe, W. Vallejo, E. Romero, M. Villareal, M. Padilla, N. Hazbun, A. Muñoz-Acevedo, E. Schott, X. Zarate, TiO2 thin films sensitization with natural dyes extracted from Bactris guineensis for photocatalytic applications: experimental and DFT study, J. Saudi Chem. Soc. 24 (2020) 407–416.

[17] A.E. Pirbazari, Sensitization of Tio2 nanoparticles with cobalt phthalocyanine: an active photocatalyst for degradation of 4-chlorophenol under visible light, Procedia Mater. Sci. 11 (2015) 622–627.

[18] Z. Youssef, L. Colombeau, N. Yesmurzayeva, F. Baros, R. Vanderesse, T. Hamieh, J. Toufaily, C. Frochot, T. Roques-Carmes, S. Acherar, Dye-sensitized nanoparticles for heterogeneous photocatalysis: cases studies with TiO2, ZnO, fullerene and graphene for water purification, Dyes Pigments 159 (2018) 49–71.

[19] R. Vinu, S. Polisetti, G. Madras, Dye sensitized visible light degradation of phenolic compounds, Chem. Eng. J. 165 (2010) 784–797.

[20] M.A. Rauf, S.S. Ashraf, Fundamental principles and application of heterogeneous photocatalytic degradation of dyes in solution, Chem. Eng. J. 151 (2009) 10–18.

[21] E. Vargas, R. Vargas, O. Núñez, A. TiO2, surface modified with copper(II) phthalocyanine-tetrasulfonic acid tetrasodium salt as a catalyst during photoinduced dichlorvos mineralization by visible solar light, Appl. Catal. B: Environ. 156 157 (2014) 8–14.

[22] S. Gorduk, O. Avciata, U. Avciata, Photocatalytic degradation of methylene blue under visible light irradiation by non-peripherally tetra substituted phthalocyanine-TiO2 nanocomposites, Inorg. Chim. Acta 471 (2018) 137–147.

[23] G.K. Upadhyay, J.K. Rajput, T.K. Pathak, P.K. Pal, L.P. Purohit, Tailoring and optimization of hybrid ZnO:TiO2:CdO nanomaterials for advance oxidation process under visible light, Appl. Surf. Sci. 509 (2020), 145326.

[24] J. Zhao, X. Yang, Photocatalytic oxidation for indoor air purification: a literature review, Build. Environ. 38 (2003) 645–654.

[25] M. Amini, M. Ashrafi, Photocatalytic degradation of some organic dyes under solar light irradiation using TiO2 and ZnO nanoparticles, Nanochem. Res. 1 (2016) 79–86.

[26] Z. Guo, B. Chen, J. Mu, M. Zhang, P. Zhang, Z. Zhang, J. Wang, X. Zhang, Y. Sun, C. Shao, Y. Liu, Iron phthalocyanine/TiO2 nanofiber heterostructures with enhanced visible photocatalytic activity assisted with H2O2, J. Hazard. Mater. 219–220 (2012) 156–163.

[27] A.D. Gülmez, M.S. Polyakov, V.V. Volchek, S.T. Kostakoğlu, A.A. Esenpinar, T. V. Basova, M. Durmuş, A.G. Gürek, V. Ahsen, H.A. Banimuslem, A.K. Hassan, Tetrasubstituted copper phthalocyanines: correlation between liquid crystalline properties, films alignment and sensing properties, Sens. Actuators B: Chem. 241 (2017) 364–375.

[28] J.C. Bommer, J.D. Spikes, Phthalocyanines: properties and applications, Photochem. Photobiol. 53 (1991), 419-419.

[29] J. Fei, Z. Han, Y. Deng, T. Wang, J. Zhao, C. Wang, X. Zhao, Enhanced photocatalytic performance of iron phthalocyanine/TiO2 heterostructure at joint fibrous interfaces, Colloids Surf. A: Physicochem. Eng. Asp. 625 (2021), 126901.

[30] K. Tekintas, Ö. Kesmez, O. Bekircan, E.T. Saka, Preparation, characterization and photocatalytic activity of novel 1,2,4-triazole based Cu(II) and Zn(II) phthalocyanines modified TiO2 nanoparticles, J. Mol. Struct. 1248 (2022), 131405.

[31] X. Li, T. Zhang, Y. Chen, Y. Fu, J. Su, L. Guo, Hybrid nanostructured Copper(II) phthalocyanine/TiO2 films with efficient photoelectrochemical performance, Chem. Eng. J. 382 (2020), 122783.

[32] R. Seoudi, G.S. El-Bahy, Z.A. El Sayed, FTIR, TGA and DC electrical conductivity studies of phthalocyanine and its complexes, J. Mol. Struct. 753 (2005) 119–126.

[33] S. Samsami, M. Mohamadizaniani, M.-H. Sarrafzadeh, E.R. Rene, M. Firoozbahr, Recent advances in the treatment of dye-containing wastewater from textile industries: overview and perspectives, Process Saf. Environ. Prot. 143 (2020) 138–163.

[34] D.A. Yaseen, M. Scholz, Textile dye wastewater characteristics and constituents of synthetic effluents: a critical review, Int. J. Environ. Sci. Technol. 16 (2019) 1193–1226.

[35] S.A. Avlonitis, I. Poulios, D. Sotiriou, M. Pappas, K. Moutesidis, Simulated cotton dye effluents treatment and reuse by nanofiltration, Desalination 221 (2008) 259–267.

[36] M.C. Tomei, J. Soria Pascual, D. Mosca Angelucci, Analysing performance of real textile wastewater bio-decolourization under different reaction environments, J. Clean. Prod. 129 (2016) 468–477.

[37] S. Noonpui, P. Thiravetyan, Treatment of reactive azo dye from textile wastewater by burhead (Echinodorus cordifolius L.) in constructed wetland: effect of molecular size, J. Environ. Sci. Health Part A 46 (2011) 709–714.

[38] K.P. Priyanka, S. Sankararaman, K.M. Balakrishna, T. Varghese, Enhanced visible light photocatalysis using TiO2/phthalocyanine nanocomposites for the degradation of selected industrial dyes, J. Alloy. Compd. 720 (2017) 541–549.

[39] L. Lutterotti, S. Matthies, H.R. Wenk, A.S. Schultz, J.W. Richardson, Combined texture and structure analysis of deformed limestone from time-of-flight neutron diffraction spectra, J. Appl. Phys. 81 (1997) 594–600.

[40] F.T.L. Muniz, M.A.R. Miranda, C. Morilla dos Santos, J.M. Sasaki, The Scherrer equation and the dynamical theory of X-ray diffraction, Acta Crystallogr. Sect. A 72 (2016) 385–390.

[41] M. Rehan, X. Lai, G.M. Kale, Hydrothermal synthesis of titanium dioxide nanoparticles studied employing in situ energy dispersive X-ray diffraction, CrystEngComm 13 (2011) 3725–3732.

[42] R. Prabakaran, R. Kesavamoorthy, G.L.N. Reddy, F.P. Xavier, Structural investigation of copper phthalocyanine thin films using X-Ray diffraction, Raman Scatt. Opt. Absorpt. Meas. Phys. Status Solidi (b) 229 (2002) 1175–1186.

[43] B. Tunhoo, J. Nukeaw, Optical properties and structure of copper (II) phthalocyanine(CuPc) organic thin film grown by electron –beam evaporation technique, in: Proceedings of the 2nd IEEE International Conference on Nano/Micro Engineered and Molecular Systems, 2007, pp. 764–767.

[44] F. Lu, M. Bao, C. Ma, X. Zhang, D.P. Arnold, J. Jiang, Infrared spectra of phthalocyanine and naphthalocyanine in sandwich-type (na)phthalocyaninato and porphyrinato rare earth complexes. Part 3. The effects of substituents and molecular symmetry on the infrared characteristics of phthalocyanine in bis (phthalocyaninato) rare earth complexes, Spectrochim. Acta Part A: Mol. Biomol. Spectrosc. 59 (2003) 3273–3286.

[45] C. BethelAnucha, I. Altin, E. Bacaksiz, I. Degirmencioglu, T. Kucukomeroglu, S. Yılmaz, V.N. Stathopoulos, Immobilized TiO2/ZnO sensitized copper (II) phthalocyanine heterostructure for the degradation of ibuprofen under UV irradiation, Separations 8 (2021).

[46] M.C. Zurita Ares, E. Villa González, A.I. Torres Gómez, J.M. Fernández, An easy method to estimate the concentration of mineral pigments in colored mortars, Dyes Pigments 101 (2014) 329–337.

[47] E. Lobry, F. Jasinski, M. Penconi, A. Chemtob, C. Ley, C. Croutxé-Barghorn, E. Oliveros, A.M. Braun, A. Criqui, Absorption and scattering in concentrated monomer miniemulsions: static and dynamic investigations, Macromol. Chem. Phys. 215 (2014) 1201–1211.

[48] L. Yang, B. Kruse, Revised Kubelka–Munk theory. I. Theory and application, J. Opt. Soc. Am. A 21 (2004) 1933–1941.

[49] J. Shen, Y. Li, J.-H. He, On the Kubelka–Munk absorption coefficient, Dyes Pigments 127 (2016) 187–188.
[50] I.K. Konstantinou, T.A. Albanis, TiO2-assisted photocatalytic degradation of azo dyes in aqueous solution: kinetic and mechanistic investigations: a review, Appl. Catal. B: Environ. 49 (2004) 1–14.
[51] M. Arami, N.Y. Limaee, N.M. Mahmoodi, N.S. Tabrizi, Equilibrium and kinetics studies for the adsorption of direct and acid dyes from aqueous solution by soy meal hull, J. Hazard. Mater. 135 (2006) 171–179.
[52] M. Faraji, N. Mohaghegh, Ag/TiO2-nanotube plates coated with reduced graphene oxide as photocatalysts, Surf. Coat. Technol. 288 (2016) 144–150.
[53] G. Qin, Q. Wu, Z. Sun, Y. Wang, J. Luo, S. Xue, Enhanced photoelectrocatalytic degradation of phenols with bifunctionalized dye-sensitized TiO2 film, J. Hazard. Mater. 199–200 (2012) 226–232.